Available online at www.sciencedirect.com
SCIENCE DIRECT®
Journal of Luminescence 121 (2006) 137–148
JOURNAL OF LUMINESCENCE
www.elsevier.com/locate/jlumin

Luminescence study of the $4f^2 5d$ configuration of Nd^{3+} in $LiYF_4$, $LiLuF_4$ and BaY_2F_8 crystals

A.F.H. Librantz[a,*], L. Gomes[a], S.L. Baldochi[a], I.M. Ranieri[a], G.E. Brito[b]

[a]*Centro de Lasers e Aplicações, IPEN-SP, Travessa R 400, Cidade Universitária, Caixa Postal 11049, CEP 05422-970, São Paulo, Brazil*
[b]*Departamento de Cristalografia, Instituto de Física, Universidade de São Paulo, Brazil*

Received 18 March 2005; accepted 16 November 2005
Available online 4 January 2006

Abstract

Ultraviolet fluorescence of Nd^{3+} ions induced by triphotonic excitation process was studied in Nd-doped $LiYF_4$, $LiLuF_4$ and BaY_2F_8 crystals using a technique of time-resolved spectroscopy. The observed ultraviolet luminescence was due to transitions between the bottom of $4f^2 5d$ configuration and $4f^3$ states of Nd^{3+} ions. Narrow emission lines superposed to the broadband emissions were observed. A detailed analysis of luminescence spectrum revealed that the narrow emissions are due to parity and spin allowed radiative transitions from the Stark levels of $^4K_{11/2}(5d)$ state created by the electrostatic interaction between the $5d$ electron and the two electrons of the $4f^2$ configuration. The narrow emissions are related to the high spin state ($S = 3/2$) which gives f–f characteristics to the f–d broadband emissions. The narrow emissions superposed to the wide emission correspond to 18%, 34% and 43% of the integrated broadband emission at 262 nm observed in $LiYF_4$, $LiLuF_4$ and BaY_2F_8 crystals, respectively. Although the $5d$–$4f^2$ interaction is observed to be weaker than $5d$-crystal field interaction, it is stronger enough to select only the radiative transitions from $4f^2 5d$ configuration to $4f^3$ states that preserves the total spin $S = 3/2$.

PACS: 78.50; 78.55; 71.55

Keywords: Time-resolved spectroscopy; Fast UV luminescence of Nd^{3+} ions; Multiphotonic laser excitation; Triphotonic excitation spectrum of $4f^2 5d$ configuration; Fluoride crystals

1. Introduction

Many fluoride crystals doped with Nd^{3+} have been recently used in the optical spectroscopy study in high energy, as the vacuum ultraviolet (VUV) and ultraviolet (UV) regions [1]. The study of the $4f^{N-1}5d \rightarrow 4f^N$ transitions of the trivalent

*Corresponding author. Tel.: +55 11 38169319; fax: +55 11 38169315.
E-mail address: lgomes@ipen.br (L. Gomes).

0022-2313/$ - see front matter © 2005 Elsevier B.V. All rights reserved.
doi:10.1016/j.jlumin.2005.11.004

ions is very important in order to extend the knowledge of the optical properties of triply ionized rare earths (RE^{3+}) to UV and VUV region. Many RE^{3+} ions among them Ce^{3+}, Pr^{3+}, Nd^{3+}, Tm^{3+} and Ho^{3+} have fast (or allowed dipole transitions) UV and VUV luminescence due to the $5d$–$4f$ interconfigurational transitions [2]. Ce^{3+} in $LiYF_4$ crystal, for example, has d–f laser emission around 320 nm with a potential wavelength tunability extending over some 30 nm. Pr^{3+} in $LiYF_4$ has laser emission at 240 nm with a bandwidth of 40 nm, while Nd^{3+} has three potentials laser emissions in the UV [2].

Recently, the UV and VUV fluorescence of RE^{3+} ions in solids has been intensively investigated because of the growing applications in this spectral range, such as generating and detecting VUV radiation [3,4]. The UV and VUV fluorescence have been investigated in heavy [5] and light lanthanides in fluoride crystals [6]. The *d–f* luminescence of Nd^{3+} is usually located in the VUV below 200 nm, and for that reason Nd-doped fluoride compounds have been studied as potential candidate for laser emission generation in the ultraviolet and vacuum ultraviolet region [7,8]. Three distinct emission bands of Nd^{3+} with decay time of ~35 ns are present in the VUV and UV range in fluoride crystals. These emissions are parity allowed radiative transitions from the lowest excited state of $4f^2 5d$ configuration ($^4K_{11/2}(5d)$) to lower levels of the $4f^3$ configuration that preserves the total spin $S = 3/2$ (or spin allowed transitions), as the ^4I_J ($J = 9/2$, 11/2, 13/2), ^4G_J ($J = 5/2$, 7/2) and ^4F_J ($J = 3/2$, 5/2) states [9]. These broadband emissions has maximums at 184, 230 and 262 nm in $LiYF_4$ measured at 300 K. Nd-doped fluoride crystals may allow the construction of the first solid-state tunable UV lasers based on the fast wide emissions of Nd^{3+} sequentially pumped by two-photon (355 nm) [10] or three-photon excitation (520 nm) [11,12], although the direct pumping with fluorine laser at 157 nm being more efficient. The triphotonic excitation of the $4f^2 5d$ (Nd^{3+}) configuration is based on a high intensity laser pumping in the visible (green) and has the advantage to match the second harmonic of Nd:YAG laser (532 nm), which is one of the most disseminated laser for optical pumping systems. The $4f^n \leftrightarrow 4f^{n-1}5d$ transition is parity allowed transition exhibiting a measured fluorescence lifetime of 25–35 ns in Nd-doped fluoride crystals. They are characterized by a stronger environmental interaction and a broadband absorption and emission spectra in the UV range with oscillator strength much higher ($>10^3$) than the one involved in the $4f^N$ internal transitions. On the other hand, the $4f^N \rightarrow 4f^N$ transitions are parity forbidden and composed by narrow lines of weak strengths mostly due to the forced electric-dipole interaction induced by odd terms of the local crystal field [13].

The $5d$–$4f$ emission bands are much wider than the multiplet emission spectrum due to $4f^2 \rightarrow 4f^2$ transitions of Pr^{3+} that are mostly in the visible near 500 nm [9]. Wide emissions and broadband absorptions are typical for the $5d$–$4f \rightarrow 4f$ transitions due to the strong coupling between $5d$ electron with the lattice phonons. An additional effect is the Stark splitting of the $4f^{N-1}$–$5d$ multiplets by the crystal field interaction, which may result in a structured UV emission band. Usually, the Stark splitting is not observed in the $5d$–$4f$ emission spectrum of light lanthanides but it does contributes to the broadening of the emission bands [6,9].

The spectrum characterization of the $4f^3 \rightarrow 4f^2 5d$ and $4f^3 \rightarrow 4f^3$ transitions of Nd^{3+} provides information about the local level structure and electron-phonon coupling differences between $4f^3$ and the $4f^2 5d$ electronic configurations because the crystal-field perturbation strength is stronger for electrons in $5d$ orbital than for those in $4f^{N-1}$ state [14]. This results in a broadband transition with a large Stokes' shift of the emission band and a high probability for phonon-assisted transitions. It was shown that the structure of the $4f^3 \leftrightarrow 4f^2 5d$ excitation and emission bands of heavier lanthanides could be explained by an extension of the established models for the $4f^N$ configuration including the crystal field and spin-orbit interactions with $5d$ electron [15–18].

An energy difference between the lowest absorption band of the $^4I_{9/2} \rightarrow 4f^2 5d$ transition centered at 175 nm [8,16] and the highest emission band from the bottom of the $4f^2 5d$ to the ($^4I_{9/2}$, $^4I_{11/2}$) states with maximum at 182 nm observed in Nd-doped

YLF has been reported [12]. This effect might be produced by the lattice relaxation of neighboring ions around the excited Nd^{3+} into the $4f^25d$ configuration in order to decreases the total energy of the system [12]. An energy of $\sim 2000\,cm^{-1}$ is dissipated by multiphonon emission by the lattice relaxation to produce the relaxed excited state (RES) of $4f^25d$ configuration located at $\sim 55{,}500\,cm^{-1}$ for Nd:YLF [12]. In this work we show that the dissipated energy is $3250\,cm^{-1}$ for the case of Nd^{3+} (5d) in BaY_2F_8 crystal.

The position of $4f^25d$ energy levels of free Nd^{3+} ion has not been determined yet from gaseous spectra, but it has been estimated using the available data of the isoelectronic Pr^{2+} ion in the $4f^25d$ configuration [19,20]. A decomposition of the $4f^25d$ configuration of Nd^{3+} gives rise to 107 ($^{2S+1}L(5d)$) levels that split into 910 ($^{2S+1}L_J$) manifolds after considering the spin–orbit interaction [21]. The $^4K_{11/2}(5d)$ state has been indicated as the lowest state of the $4f^25d$ configuration of Nd^{3+} [8,22]. Recent experimental and theoretical developments have been made to describe the *f–d* excitation spectrum of light lanthanides ($N<7$) in three host lattices (YPO_4, CaF_2 and YLF) [6]. In this article, the *f–d* excitation spectrum of Ce^{3+} ion was used as probe of the crystal-field splitting and spin-orbit parameters of 5*d* electron in new hosts than LaF_3. The 5*d* electron ($l=2$) in the S_4 symmetry of YLF host splits into four states Γ_1, $2\Gamma_2$, Γ_3 and Γ_4 according to the group theory (using Bethe's notation). Each one of these irreducible representations gives rise to a broad excitation band in the UV and VUV range due to $4f \rightarrow 5d$ transition of Ce^{3+} in YLF crystal. Pieterson et al. [6] observed a similar *f–d* excitation bands due to the crystal-field splitting and spin-orbit coupling for Pr^{3+}, Nd^{3+}, Sm^{3+} and Eu^{3+} in the same host lattice. They conclude that the electronic states produced by the crystal–field interaction with the 5*d*-electron dominates the structure in the *f–d* excitation spectra, even in the more complex (rare-earth ions with more than one 4*f* electron) cases i.e., broadband with the presence of zero phonon lines seen at low temperatures, which is characteristic of vibronic transitions [15]. The contribution of $4f^{N-1}$–5*d* Coulomb interaction could add some narrowest structures but it has not been observed yet. In the case of Nd^{3+} in YLF, it has been observed that the $4f^2$–5*d* Coulomb interaction parameter was reduced to 74% of the one calculated for the free ion [6]. However, the crystal field parameters of 5*d*-electron was 98% of one obtained for Ce^{3+}. This means that the 5*d*-electron stronger interacts with the crystal field lattice than with the electrons of $4f^2$ configuration in light lanthanides (as the case of Nd^{3+}).

2. Experimental procedure

Single crystals doped with neodymium were grown by the Czochralski technique under a purified argon atmosphere [23]. The starting growth material was doped with 3 mol % of Nd in the case of $LiYF_4$ (YLF) and $LiLuF_4$ (LLF) and 2 mol % in the case of BaY_2F_8 (BaYF). The Nd^{3+} concentration inside of the crystal was 1.3 mol % for YLF and LLF, and 1.6 mol % in the case of BaYF, all determined by X-ray fluorescence technique. Ultra pure LiF and fluorides YF_3, BaF_2 and NdF_3 were obtained by hydrofluorination from commercial Y_2O_3, $BaCO_3$ and Nd_2O_3 (99.99%) and used as the starting materials for the crystal growth. The YLF and LLF samples were cut and polished properly with the *c*-axis parallel to the longest side of the rectangular faced samples for YLF and LLF crystals. The BaYF crystal growth first in the zone refining system was oriented on an adjustable mount using the back-reflection Laue patterns of an incident X-ray beam, and then cut and polished with *b*-axis parallel to the longest side of the rectangular faced sample to produce an oriented crystal to work as a seed to grow an oriented crystal for the crystal growth system.

A time-resolved spectroscopy system of 1 ns of time resolution provided the emission spectra discrimination and the decay time determination. The laser pumping system consists of an optical parametric oscillator (OPO) from OPOTEK pumped by the third harmonic of the Nd:YAG (355 nm) laser Brilliant B from QUANTEL. Laser tunability in the visible range from 420 to 680 nm delivers a typical energy of 20 mJ with a repetition

rate of 10 Hz and a pulse duration of 4 ns. For the measurements in 300–120 nm range we use a VUV 0.67 m monochromator from McPherson, model 207 V, coupled to a vacuum system composed by mechanical and turbo-molecular pumps generating a vacuum of $\sim 1 \times 10^{-5}$ Torr. Luminescence signals were detected by a HAMAMATSU solar blind photomultiplier tube type R7311 with a time response of 1 ns (at 50 Ω) and sealed with a MgF_2 small window. A signal processor EGG/PAR 4402 model with box-car averager computer interfaced by the GPIB port was used to temporally discriminate the luminescence signals. In order to maximize the signal/noise ratio of VUV luminescence, the sample was fixed in the copper sample holder inside of a vacuum chamber having two quartzes optical windows that allows the laser excitation. A crossing exit of the sample chamber was attached to the VUV monochromator entrance. A small CaF_2 lens placed inside of the sample chamber between the sample and the slit of the monochromator was used to collect the luminescence. A vacuum of 1×10^{-5} Torr was made inside of the detecting system including the sample chamber and the monochromator to avoid luminescence intensity attenuation by the presence of oxygen and nitrogen gas component of the air.

The luminescence spectrum was time resolved and discriminated using the box-car averager that operates in static gate mode with a sample point (SP) of 20 ns to measure the fast luminescence and SP = 1 μs the slow component of the UV luminescence signal. Luminescence lifetime was measured using a digital oscilloscope of 100 MS/s model TDS410 from TEKTRONIX. Both equipments are interfaced to a microcomputer. In all the luminescence experiments the laser excitation beam was slightly focused in the sample exhibiting a spot of $\sim 0.5\,mm^2$ and a typical energy of 10 mJ to avoid the crystal damage and to minimize the crystal stress that scatters the UV luminescence and therefore decreases the signal to noise ratio. The laser induced up conversion luminescence technique and the luminescence analysis system used in this work contributed for the luminescence signals enhancement and an adequate signal to noise ratio, which allowed a spectral resolution of 0.05 nm in the UV range.

3. Experimental results and discussion

3.1. Triphotonic excitation process

According to our previous results on the investigation of the multiphotonic excitation process of $4f^2 5d$ configuration of Nd^{3+} in YLF and LLF crystals induced by pulsed laser excitations in the visible spectral range [12], the following excitation sequences leaded to the excitation of the first and the second bands of the $4f^2 5d$ configuration of Nd^{3+} in YLF, LLF and BaYF crystals:

Process 1:

$$^4I_{9/2} + h\nu' \rightarrow (^4G_{7/2}, ^4G_{9/2}, ^2K_{13/2}) + h\nu' \rightarrow {}^2F(2)_{5/2} + h\nu' + 4f^2 5d\,(1st)$$

($h\nu'$ = laser excitation in the green),

Process 2:

$$^4I_{9/2} + h\nu'' \rightarrow {}^2G(1)_{9/2} + h\nu'' \rightarrow {}^2F(2)_{7/2} + h\nu'' + 4f^2 5d\,(2nd)$$

($h\nu''$ = laser excitation in the blue).

The $4f^2 5d$ configuration was attained after three sequential stepwise excitations occurring during a single pulse laser application as illustrated in Fig. 1 for Nd^{3+} in YLF crystal. The energy levels of $4f^3$ states were obtained from Refs. [24,25]. Using tunable laser excitations in the visible range from an OPO laser with delivers pulse energy of 10 mJ (4 ns) we could efficiently excite the $4f^2 5d$ electronic configuration of Nd^{3+} in YLF, LLF and BaYF [26]. The excitation spectrum of the fast UV luminescence (35 ns) was measured by monitoring the fast UV luminescence intensity at 262 nm using the box-car averager operating in the static gate mode with a sample point (SP) of 20 ns and gate width of 2 ns tuned in the visible range (green to blue). Tunable laser excitations produced by the OPO system in the visible range were used to excite Nd^{3+} ions to the $^2F(2)_{5/2}$ state of $4f^3$ configuration by two photon absorptions and the $^4K_{11/2}(5d)$ (first) and $^4I_{9/2}(5d)$ (second) excited states of $4f^2 5d$ configuration by three photon absorptions. Pulsed laser excitation in the green region excites Nd^{3+} ions exclusively to the lowest state of $4f^2 5d$ configuration (first excitation band) located at

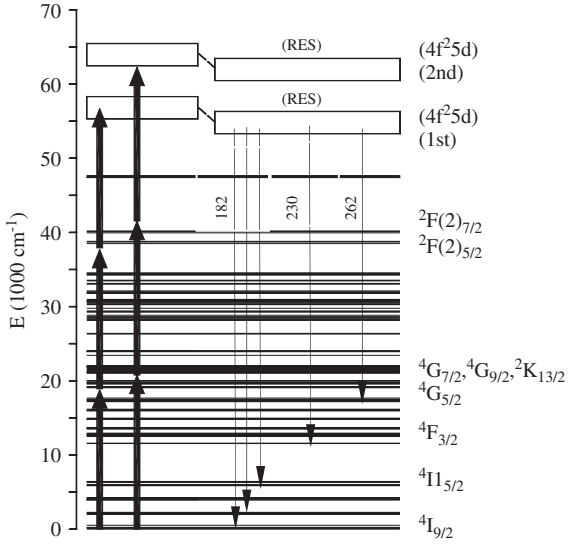

Fig. 1. Schematic diagram of the energy levels of Nd^{3+} ions in YLF showing the triphotonic excitation processes and the fast UV luminescence from the bottom of the $4f^25d$ configuration. The levels positions, as well the Stoke's shift were obtained from Refs. [22,23].

55,500 cm^{-1} in YLF. The excitation spectrum of one photon process has been measured using synchrotron radiation [15,16]. The $^4K_{11/2}(5d)$ (or $4f^2(^3H)5d$) state has been indicated as the lowest state of the $4f^25d$ configuration of Nd^{3+} [8,22]. On the other hand, the excitation in the blue spectral region excites primarily the $^4I_{9/2}(5d)$(or$4f^2(^3G)5d$) state whose population is nonradiatively transferred to the bottom of the $4f^25d$ configuration. It is important to observe that the laser intensity used in this experiment was typically in the order of 2×10^8 W/cm^2, which is well below the threshold intensity for color center formation in fluoride crystals that has been estimated to be in the order of 2×10^{13} W/cm^2 [27]. Indeed we have not found the existence of color center absorption after laser irradiation in pure and Nd-doped YLF, LLF and BaYF crystals. The excitation spectrum of the $4f^25d$ configuration of the Nd^{3+} in BaYF was measured by monitoring the 262 nm fast emission using two laser excitation symmetries. In the first case, the crystal was placed with *b*-axis parallel to laser electric field (π-polarization). In other case, the crystal was positioned with the *b*-axis perpendicular to the laser or σ-polarization. The excitation spectra measured in π and σ polarization is showed in Fig. 2. Two well separated excitation bands in the green and blue region composed by narrow excitation lines were observed. However, both green and blue excitation spectra do not exhibit accentuated difference for two polarization symmetries used. This may be caused by the crystal symmetry of BaYF that has three crystalline axes distinct ($a\neq b\neq c$). This polarization effect is differently than one is observed for YLF and LLF crystals that have *a*- and *b*-axes equals and *c*-axis distinct [12]. Excitation spectrum of 262 nm fast emission for Nd^{3+} in YLF and LLF are shown in Fig. 3.

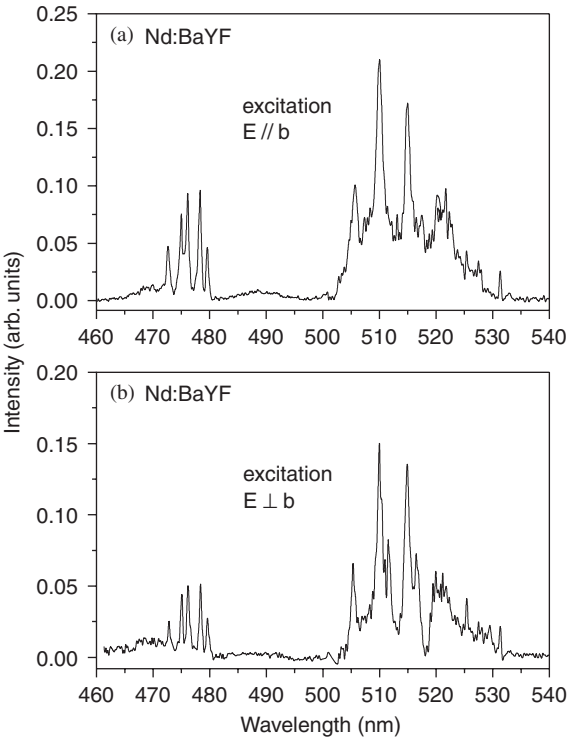

Fig. 2. Excitation spectra of the first and second band of the $4f^25d$ configuration of Nd^{3+} in BaY_2F_8 crystal measured at 300 K with *b*-axis perpendicular to the laser electric field ($E\perp b$) (or σ-polarization of Fig. 2(b)) and with $E//b$ (π-polarization) exhibited in Fig. 2(a). Laser excitations with 10 mJ per pulse and 4 ns of time duration with a 10 Hz of repetition rate were used to induce the 262 nm fast emissions. The abscissa represents the wavelength of laser excitation continuously tuned using the Nd:YAG laser (3 W) pumped OPO.

The mean excitation energy involved in the thriphotonic process was calculated by multiplying the mean photon energy of the barycenter of the green excitation spectrum by a factor of three. This means excitation energy was compared to the highest photon energy emitted from the bottom of the $4f^2 5d$ configuration for comparison. An energy difference of 2000, 2050 and 3250 cm^{-1} were, respectively, found in YLF, LLF and BaYF crystals. The largest energy difference was observed in BaYF crystal, which is consistent with the fact its crystalline field is stronger than that of YLF and LLF crystals. Perhaps, a stronger lattice relaxation affects the total energy of the $4f^2 5d$ configuration that goes to the relaxed excited state (RES) from where all the emission occurs.

Fig. 4 shows the second photon absorption spectrum expected in the green region and calculated for Nd^{3+} in YLF crystals by using the energy levels data from Ref. [22]. The x-coordinate

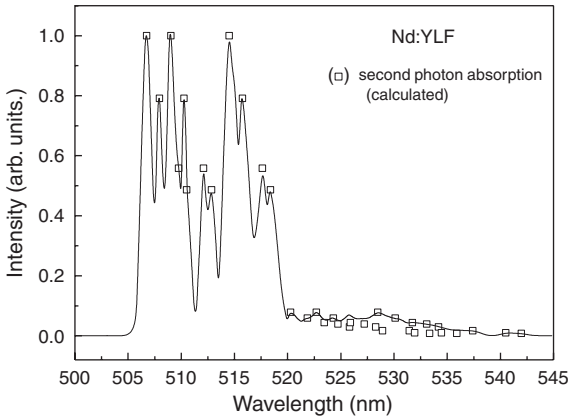

Fig. 4. Calculated spectrum of the second photon absorption involving all the expected transitions from the $^4G_{7/2}$, $^4G_{9/2}$ and $^2K_{13/2}$ excited states reached after the one photon absorption in the green region, to the $^2F(2)_{5/2}$ excited state of Nd^{3+} in YLF crystal. Open squares represents all the expected transitions calculated from the energy difference between the initial and final states. Solid line represents the envelop obtained assuming that all the transition lines have a Gaussian shape of 1 nm of half width.

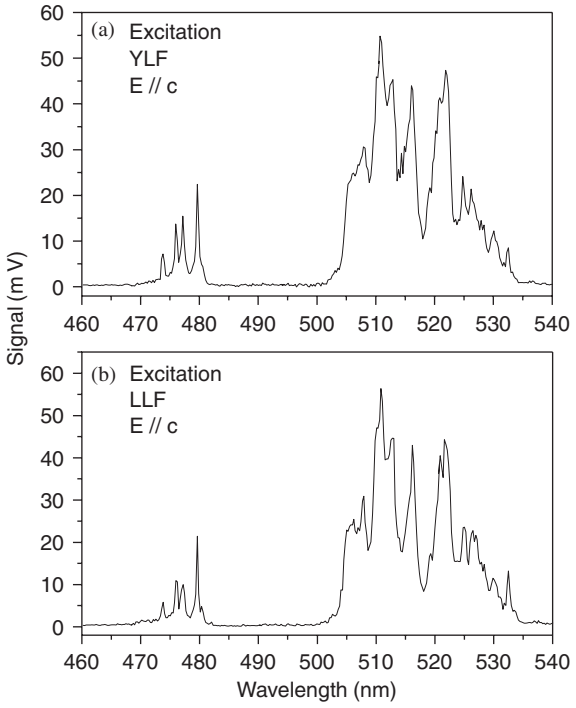

Fig. 3. Measured excitation spectra of Nd^{3+} in YLF and LLF crystals with the c-axis placed parallel to the electric field ($E//c$) of the laser excitation that has a mean energy of 10 mJ at 300 K by monitoring the fast UV luminescence of 35 ns at 262 nm.

assigned by open squares gives the wavelength of ($^4G_{7/2}$, $^4G_{9/2}$, $^2K_{13/2}$)→$^2F(2)_{5/2}$ Stark transitions. On the other hand, the y-coordinate gives the relative intensity of the transitions obtained by the Boltzmann distribution applied to the Stark levels of the initial states only. The envelope curve (solid line) in Fig. 4 represents the second photon absorption spectrum calculated assuming a Gaussian function with 1 nm (half-width) for each transition line. This result shows that the measured excitation spectrum exhibited in Fig. 3(a) matches the absorption band expected for the ($^4G_{7/2}$, $^4G_{9/2}$, $^2K_{13/2}$)→$^2F(2)_{5/2}$ transition involved in the second step of triphotonic excitation process of Nd^{3+} in YLF. The verified power law dependence ($b = 2.85$) for the 262 nm fast emission (35 ns) exhibited in Fig. 5 indicates that the laser induced fast UV emissions are due to photonic process of third order.

3.2. Narrow structures observed in the UV broad emission

In Fig. 6, it was shown the fast UV emission (35 ns) spectra of Nd^{3+} in BaYF and YLF crystals

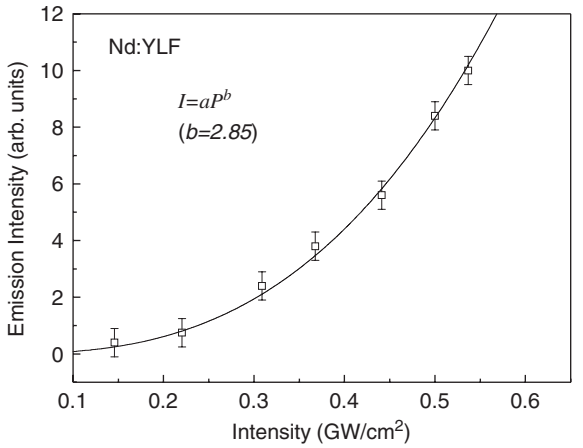

Fig. 5. This figure shows the experimental measurement of the 262 nm emission (35 ns) dependence on the laser excitation intensity P(GW/cm^2) at 517 nm for Nd:YLF. Transversal area of excitation volume was estimated to be of 6×10^{-5} cm^2. The energy of laser pulse was varied while the excitation volume was kept fixed. A power factor of 2.85 was obtained indicating that a three-order process is responsible for the 262 nm fast emission.

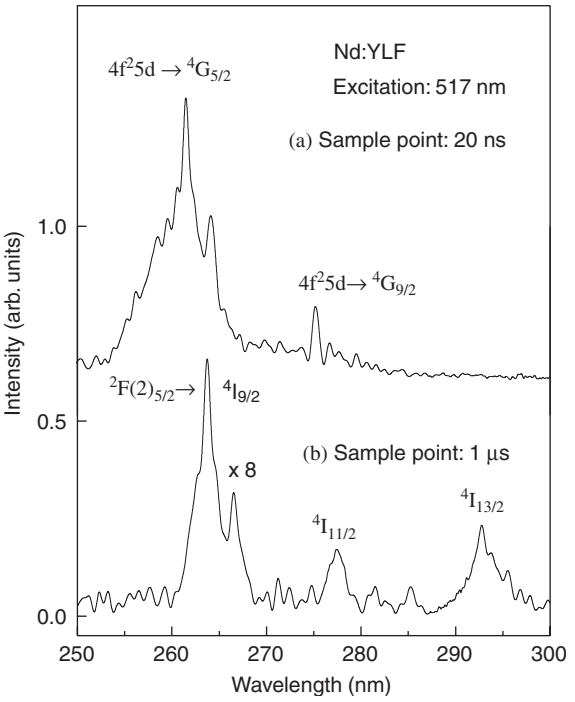

Fig. 6. UV emission bands near 262 nm measured for Nd:YLF induced by triphotonic laser excitation at 517 nm at 300 K. Luminescence signals were discriminated using a box-car averager with sample points of 20 ns (curve (a)) and 1 μs (curve (b)) with a gate width of 2 ns. Emissions exhibited by curve (b) are attributed to $^2F(2)_{5/2}$ excited level that has a measured lifetime of 8 μs. The slow emission (b) was measured with ~50 cm^{-1} of resolution, while the fast emission (a) was measured with 14 cm^{-1} of resolution.

measured at 300 K, induced by laser excitation at 517 nm ($E=10$ mJ). Narrow structures superposed to the broadband emissions are seen and better observed in the spectra shown in Fig. 9 that exhibits the luminescence intensity as a function of transition energy (cm^{-1}) for 230 and 262 nm emissions in three different crystals used. The narrow structures were assigned to localized Stark levels of $^4K_{11/2}(5d)$ state produced by the LS coupling between $5d$ and $4f^2$ electrons having a total spin $S=3/2$. These narrow emissions are interconfigurational radiative transitions from $^4K_{11/2}(5d)$ to (^4F_J, ^4G_J) states of $4f^3$ configuration preserving the total spin ($\Delta S=0$) besides the $5d$ state relaxation with its strong phonon-induced contribution to the broad emission.

The Figs. 6 and 7 show the time-resolved emission spectra around 262 nm obtained using the sample point of 20 ns (fast emission having a lifetime of 35 ns) and another using the sample point of 1 μs to measure only the slow emission from the $^2F(2)_{5/2}$ state having a lifetime of 8 μs. This 262 nm emission was induced by 517 nm laser excitation in Nd-doped YLF and BaYF crystals. By comparing spectrum (a) and spectrum (b) of both Figs. 6 and 7, one must conclude that they are originated from different electronic configurations, i.e. $4f^25d$ [$^4K_{11/2}(5d)$] and $4f^3$ ($^2F(2)_{5/2}$), respectively. Fig. 8 shows the fast UV emission bands measured from the bottom of the $4f^25d$ configuration of Nd^{3+} in BaY_2F_8 and $LiYF_4$ crystals induced by triphotonic laser excitation at 517 nm for comparison. Fig. 9 shows the 262 and 230 nm fast emission bands measured for $LiYF_4$ (a), $LuLiF_4$ (b) and BaY_2F_8 (c) crystals for comparison, were the narrow emission lines superposing the broadband emissions are seen.

In Figs. 10–12 it were shown the fast UV emission band centered at 262 nm in details to emphasize the narrow structures that are more evident in this case. In Table 1 are given the energy

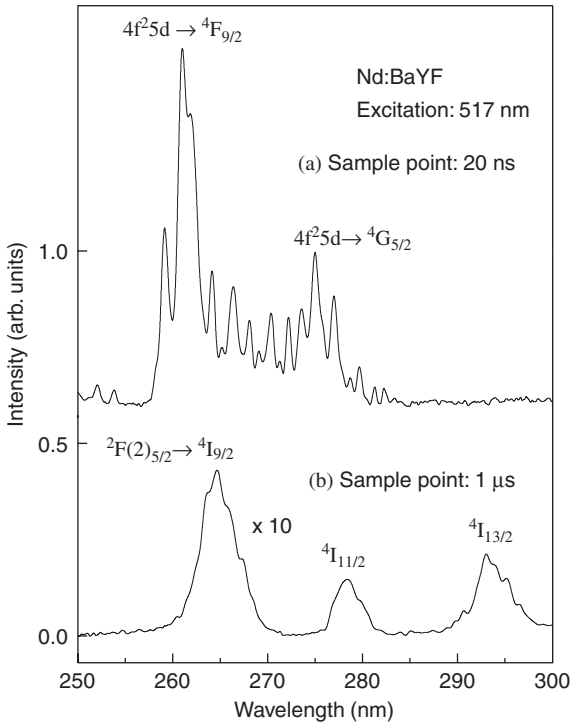

Fig. 7. UV emission bands (near 262 nm) measured for Nd:BaYF induced by triphotonic laser excitation at 517 nm at 300 K. Luminescence signals were discriminated using a box-car averager with sample points of 20 ns (curve (a)) and 1 μs (curve (b)) with a gate width of 2 ns. The slow emission (b) was measured with ~50 cm^{-1} of resolution, while the fast emission (a) was measured with 14 cm^{-1} of resolution.

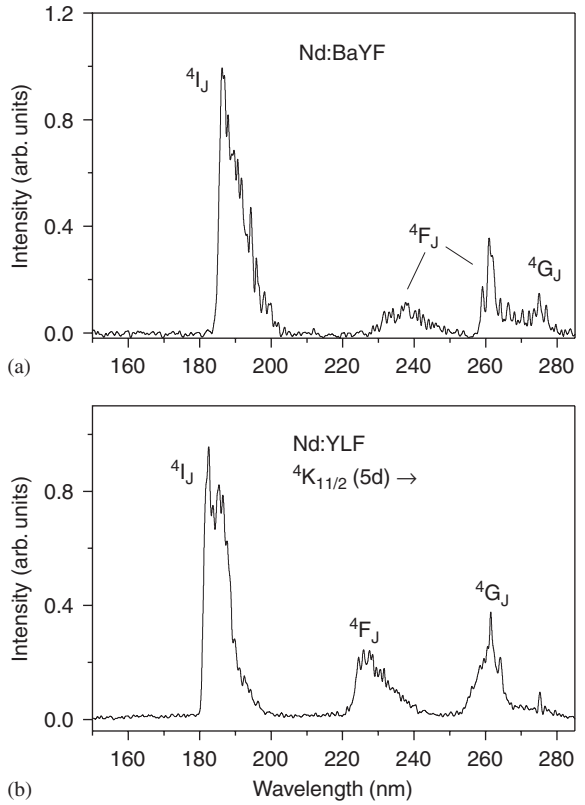

Fig. 8. Fast UV emission bands measured from the bottom of the $4f^25d$ configuration of Nd^{3+} in BaY_2F_8 and $LiYF_4$ crystals induced by triphotonic laser excitation at 517 nm with 10 mJ per pulse of 4 ns of time duration and 10 Hz (at 300 K). Luminescence signals were discriminated using a box-car averager with sample point of 20 ns and a gate width of 2 ns.

positions of these narrow emissions observed in the three crystals used.

Table 2 gives the percentage contribution of these narrow emissions in the 230 and 262 nm broadband emissions for the three crystals used. It is seen that the narrow emissions contribution (area) increases when changing the crystal host from YLF to BaYF. Perhaps this effect is dependent on the crystalline field strength felt by Nd^{3+} ion. It was observed that the structure of the 262 nm fast emission has six narrow lines in YLF and LLF crystals, which is in agreement with the number of Stark levels of the $^4K_{11/2}(5d)$ state expected for the Nd^{3+} in the S_4 symmetry (and C_2 symmetry for BaYF).

Stark level positions (E_{X_i}) of the $^4K_{11/2}(5d)$ state were calculated using Eq. (1) by assuming that the Stark splitting effects on the $^4K_{11/2}(5d)$ state is stronger than one that occur for $4f^3$ states. For instance, the maximum energy separation observed in the structures of the 262 nm fast emission in YLF (1169 cm^{-1}) is approximately 8 times larger than that observed for the $^4G_{5/2}$ state (140 cm^{-1}).

$$E_{X_i} = E_i + \langle E \rangle_{\text{low}}, \tag{1}$$

where E_{X_i} is the Stark level energy position (X_i), E_i is the narrow emission transition given in Table 1 and $\langle E \rangle_{\text{low}}$ represents the mean energy value of lower $4f^3$ state, which is $^4G_{5/2}$ for YLF and LLF situated at 17,265 cm^{-1} and the $^4F_{9/2}$ at 15,398 cm^{-1} in BaYF. In Table 3 are given the

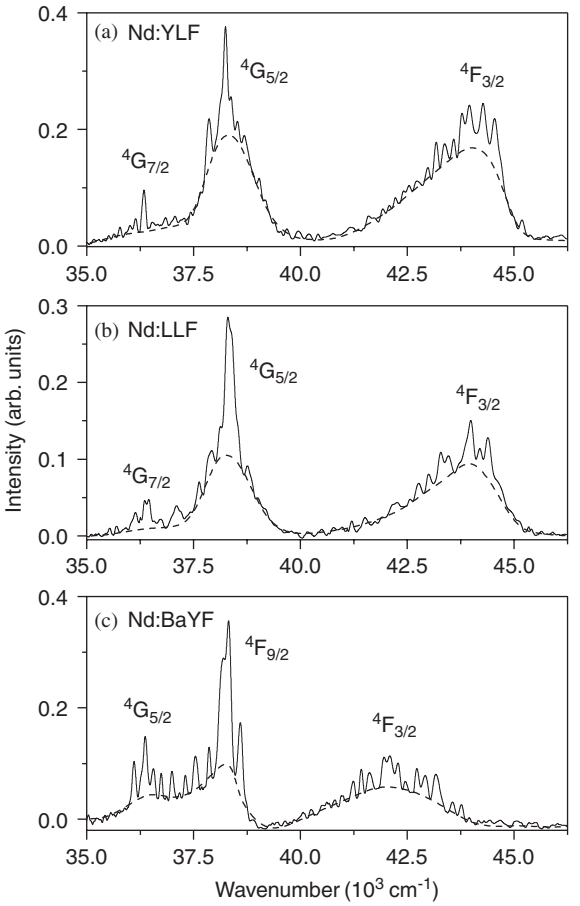

Fig. 9. Fast 262 and 230 nm emission bands from $4f^2 5d$ configuration of Nd^{3+} in $LiYF_4$ (a), $LuLiF_4$ (b) and BaY_2F_8 (c) crystals exhibited in energy scale (cm^{-1}). Narrow emission lines superposing the broadband emissions (dashed line) are seen.

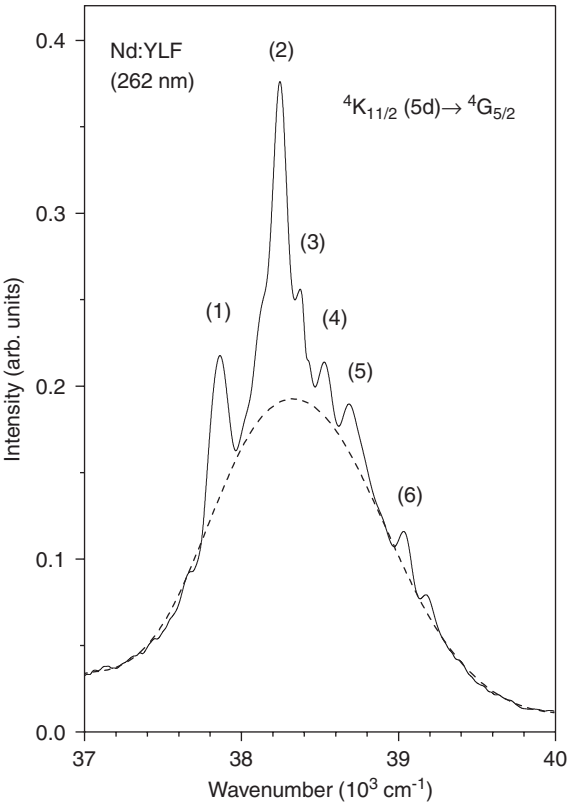

Fig. 10. Details of the 262 nm emission band due to the $4f^2 5d \rightarrow {}^4G_{5/2}$ transition observed for Nd^{3+} in $LiYF_4$ measured with high signal to noise ratio (10 samples per point). The narrow structure superposed to the broad emission represented by a Gaussian function (dashed line) is shown. Six narrow lines numbered from 1 to 6 were related to the $^4K_{11/2}(5d)$ to the $^4G_{5/2}$ state of $4f^3$ configuration.

Stark level positions of the $^4K_{11/2}(5d)$ manifold calculated using Eq. (1) for the crystals used. An interesting observation in the structure of the 262 nm fast emission is that the maximum of the broadband emission always coincides with the most intense line of narrow emissions (as seen in Figs. 10–12). This effect might indicate that the narrow emission lines should involve the $4f^2$–$5d$ coupled states in thermal equilibrium with the $5d$-lattice coupled state. A similar effect is also observed for the 230 nm emission band. The emission from the $^4K_{11/2}(5d)$ states can be distinguishable observed together with broad emission because of its larger emission cross section in comparison to the broad emission taking into account its transition width of about 10 cm^{-1} ($\sim$1190 cm^{-1} half width for 262 nm emission broad band). Besides of this, the authors state that the reason for the very different emission observed under three-step excitation compared to that previously observed under one-step excitation is not understood.

The observed effect that the $4f^2$–$5d$ fast emission from $^4K_{11/2}(5d)$ state is sharper than $4f^3$ slow emission from $^2F(2)_{5/2}$ state, exhibited in Figs. 6 and 7, is explained by the fact that the Stark

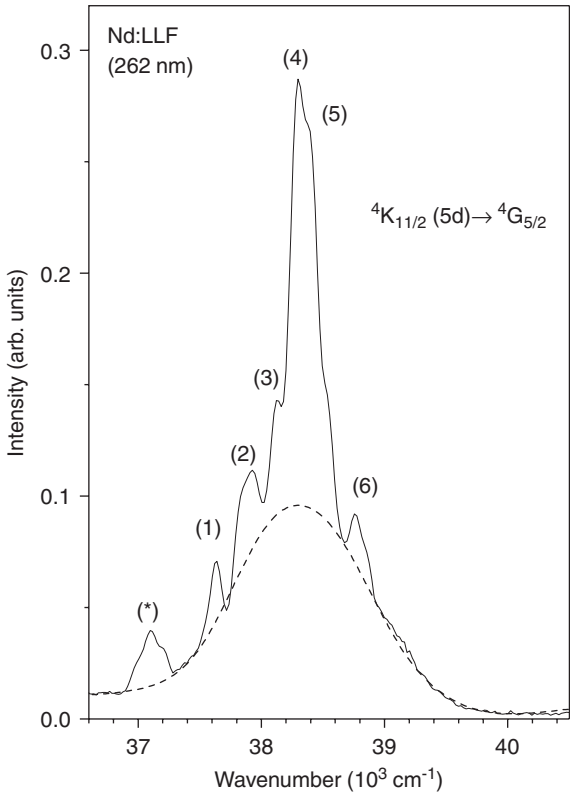

Fig. 11. Structure of the 262 nm emission from $4f^25d$ configuration of Nd^{3+} in $LiLuF_4$ crystal measured at 300 K with the high signal to noise ratio (10 samples per point). The narrow structure superposed to the broad emission represented by Gaussian function (dashed line) is shown. Six narrow lines (1–6) are related to the $^4K_{11/2}(5d)$ to the $^4G_{5/2}$ state of the $4f^3$ configuration. (*) Peak is related to the downward transition to $^4G_{7/2}$ state.

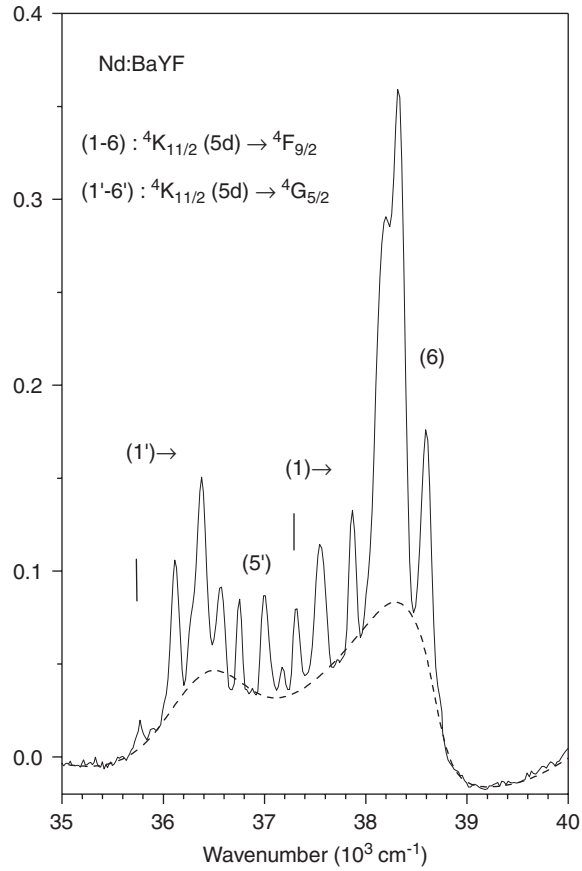

Fig. 12. Structure of the 262 nm emission of $4f^25d$ configuration of Nd^{3+} in BaY_2F_8 crystal measured at 300 K with high signal to noise ratio (10 samples per point). Narrow structures superpose to the vibronic emission represented by two Gaussian functions (dashed line). Six narrow lines (1–6) are due to downward transition to the $^4F_{9/2}$ state. On the other hand lines 1′ to 6′ are related to downward transition to the $^4G_{5/2}$ state.

splitting effect ($\Delta = 1169\,cm^{-1}$) on the former state is ~4 times more intense than the observed for the $^2F(2)_{5/2}$ state ($\Delta = 298\,cm^{-1}$). In addition, the slow UV emission was measured with smaller resolution (~50 cm^{-1}) due to the weaker luminescence signal of slow components (8 μs) (fast luminescence signals were detecting with 14 cm^{-1} of resolution).

4. Conclusions

The multiphotonic excitation process of Nd^{3+} in YLF, LLF and BaYF was investigated and a three stepwise photon excitation in the blue and green spectral range was measured and characterized. The triphotonic excitation spectrum of the $4f^25d$ configuration of Nd^{3+} in BaYF is slightly dependent on the excitation polarization in the visible range.

The VUV–UV luminescence investigations showed that only the lowest excited state of the $4f^25d$ configuration (RES) is radiative and full efficient, although the triphotonic excitation at 479 nm excites the second band located at 63,000 cm^{-1} in all the crystals used in this work. The energy difference between the first band

Table 1
Peak position (cm^{-1}) of the narrow emissions superposed to the broadband emission at 262 nm obtained from the localized states of $^4K_{11/2}(5d)$ manifold of the $4f^2 5d$ configuration of Nd^{3+} ions in YLF, LLF and BaYF crystals at 300 K

	Narrow emissions from Stark levels of $^4K_{11/2}$ ($5d$) state (cm^{-1})		
	YLF	LLF	BaYF
$^4G_{5/2}$	(1) 37,864; (2) 38,252; (3) 38,390; (4) 38,529; (5) 38,689; (6) 39,033	(1) 37,641; (2) 37,928; (3) 38,141; (4) 38,298; (5) 38,396; (6) 38,795	(1′) 35,758; (2′) 36,104; (3′) 36,368; (4′) 36,564; (5′) 36,744; (6′) 37,000
$^4F_{9/2}$	—	—	(1) 37,314; (2) 37,559; (3) 37,864; (4) 38,193; (5) 38,331; (6) 38,589

All luminescence measurements were done with the sample inside of a vacuum chamber under 1×10^{-5} Torr connected to the VUV monochromator (with an optical resolution of 0.05 nm at first order).

Table 2
Narrow emissions contributions relative to the integrated luminescence over the correspondent broad emission due to the $^4K_{11/2}(5d) \rightarrow 4f^3$ transitions measured for Nd^{3+} in YLF, LLF and BaYF crystals at 300 K

Downward transition to (emission range)	Narrow emissions contributions (%)		
	YLF	LLF	BaYF
($^4F_{3/2}$, $^4F_{5/2}$) (220–248) nm	16	18	44
($^4G_{5/2}$, $^4G_{7/2}$)	18	34	—
($^4F_{9/2}$, $^4G_{5/2}$) (255–282) nm	—	—	43

Table 3
Stark levels positions of the $^4K_{11/2}(5d)$ manifold derived from the observed narrow emissions superposed to the 262 nm broad band emission from the $4f^2 5d$ configuration of Nd^{3+} in YLF, LLF and BaYF crystals measured at 300 K

Stark level	Stark levels positions (cm^{-1})		
	YLF	LLF	BaYF
1	55,129	54,868	52,712
2	55,517	55,155	52,957
3	55,655	55,368	53,262
4	55,794	55,525	53,592
5	55,954	55,623	53,729
6	56,298	56,022	53,987

attained by the triphotonic excitation at 517 nm and the relaxed excited state of the $4f^2 5d$ configuration, from where all the fast emissions occur, were found to be 2000, 2100 and 3250 cm^{-1} for the YLF, LLF and BaYF, respectively.

Narrow structures superposed to the broadband emissions from the $4f^2 5d$ (RES) state were discriminated for the 262 nm fast emissions of YLF, LLF and BaYF crystals, showing that they are prominent of the Stark levels created by the LS coupling between $5d$ orbital and the $4f^2$ electronic configuration. A localized $^4K_{11/2}(5d)$ state is created in the bottom of the $4f^2 5d$ configuration and its effects on the emission structure increases with the crystalline field strength. YLF, LLF and BaYF crystals doped with low concentration of Nd^{3+} ions (~1 mol %) can be effectively excited by three photons in the green and blue region with an intensity below the damage threshold (2.2 GW/cm^2) and can be used as an alternative way of pumping Nd-doped fluoride materials to generate laser action at the ultraviolet region

(185, 230 and 262 nm) at room temperature. This mechanism seems to be very promising to construct a neodymium UV laser based in all solid-state components.

Acknowledgments

The authors thank the financial support from FAPESP (Grants nos. 1995/4166-0 and 2000/10986-0) and CNPq. One of the authors (A.F.H. Librantz) thanks CAPES for the fellowship.

References

[1] Y. Guyot, A. Collombert, T. Somatri, A. Tkachuk, M.F. Joubert, J. Alloys and Compounds 341 (2002) 174.
[2] M.F. Joubert, R. Moncorgé, Opt. Mater. 22 (2003) 93.
[3] E. Sarantopoulou, Z. Kollia, A.C. Cefalas, Opt. Commun. 169 (1999) 263.
[4] E. Sarantopoulou, Z. Kollia, A.C. Cefalas, Microelectron. Eng. 61–62 (2002) 133.
[5] L. van Pieterson, M.F. Reid, R.T. Wegh, S. Soverna, A. Meijerink, Phys. Rev. B 65 (2002) 045114.
[6] L. van Pieterson, M.F. Reid, G.W. Burdick, A. Meijerink, Phys. Rev. B 65 (2002) 045113.
[7] M.A. Dubinski, A.C. Cefalas, E. Sarantopoulou, S.M. Spyrou, C.A. Nicolaides, R.Yu. Abdulsabirov, S.L. Korableva, V.V. Semashko, J. Opt. Soc. Am. B 9 (1992) 1148.
[8] Y. Guyot, S. Guy, M.F. Joubert, J. Alloys Compounds 323–324 (2001) 722.
[9] P. Dorenbos, J. Luminescence 91 (2000) 106.
[10] P.W. Dooley, J. Thogersen, J.D. Gill, H.K. Haugen, R.L. Brooks, Opt. Commun. 183 (2000) 451.
[11] J. Thogersen, J.D. Gill, H.K. Haugen, Opt. Commun. 132 (1996) 83.
[12] A.F.H. Librantz, L. Gomes, L.V.G. Tarelho, I.M. Ranieri, J. Appl. Phys. 95 (4) (2004) 1681.
[13] S.K. Gayen, B.Q. Xie, J. Opt. Soc. Am. B 10 (1993) 993.
[14] F. Krupke, IEEE J. Quant. Electron. 7 (1971) 153.
[15] M.F. Reid, L. van Pieterson, R.T. Wegh, A. Meijerink, Phys. Rev. B 62 (22) (2000) 14744.
[16] A. Collombert, Y. Guyot, M.F. Joubert, M. Laroche, J. Margerie, R. Moncorgé, E. Descroix, Phys. Rev. B 68 (2003) 035115.
[17] A. Collombet, Y. Guyot, M.F. Joubert, J. Margerie, R. Moncorgé, Opt. Mater. 24 (2003) 215.
[18] A. Collombet, Y. Guyot, M.F. Joubert, J. Margeire, R. Moncorgé, A. Tkachuk, J. Opt. Soc. Am. B Opt. Phys. 21 (11) (2004) 2053.
[19] J. Sugar, J. Opt. Soc. Am. 53 (1963) 831.
[20] J. Sugar, J. Reader, J. Chem. Phys. 59 (1973) 2083.
[21] C. Pedrini, F. Gaume-Mahn, D.J. McClure, Rare Earths Mod. Sci. Technol. 3 (1982) 165.
[22] Z. Kollia, E. Sarantopoulou, A.C. Cefalas, A.K. Naumov, V.V. Semashko, R.Yu. Abdulsabirov, S.L. Korableva, Opt. Commun. 149 (1998) 386.
[23] I.M. Ranieri, et al., J. Cryst. Growth 166 (1996) 423.
[24] A.A.S. da Gama, G.F. de Sá, J. Chem. Phys. 75 (1981) 2583.
[25] R.T. Wegh, A. Meijerink, R.J. Lamminmaki, J. Holsa, J. Lumin. 87 (2000) 1002.
[26] A.F.H. Librantz, Investigation of multiphotonic excitation processes of the $4f^2 5d$ configuration of Nd^{3+} in fluoride crystals, Ph.D. thesis, University of São Paulo, Brazil, 2004.
[27] L.C. Courrol, R.E. Samad, L. Gomes, I.M. Ranieri, S.L. Baldochi, N.D. Vieira Jr., Opt. Express 12 (2) (2004) 288.